Desalination and Water Treatment
www.deswater.com

doi: 10.5004/dwt.2021.26478

209 (2021) 289–301
January

Tetracycline adsorption from aqueous solutions by a magnetic nanoadsorbent modified with ionic liquid

Ruhollah Kasraei[a,b], Mohammad Malakootian[a,b,*]

[a]*Environmental Health Engineering Research Center, Kerman University of Medical Sciences, Kerman, Iran, Tel. +(98)3431325128; Fax: +(98)3431325105; emails: m.malakootian@yahoo.com/m_malakootian@kmu.ac.ir (M. Malakootian), krouhallah@gmail.com (R. Kasraei)*

[b]*Department of Environmental Health Engineering, School of Public Health, Kerman University of Medical Sciences, Kerman, Iran*

Received 26 October 2019; Accepted 24 August 2020

ABSTRACT

Removal of tetracycline (TC) by the adsorption process was investigated by using iron oxide nanoparticles (Fe_3O_4 NP) modified with the trioctylmethylammonium thiosalicylate (TOMATS) ionic liquid (IL) (Fe_3O_4 NP@TOMATS IL) as a new magnetic nanoadsorbent. The adsorbent was characterized by field-emission scanning electron microscopy–energy-dispersive X-ray spectroscopy, Fourier-transform infrared, Brunauer–Emmett–Teller, and X-ray diffraction. Batch experiments were carried out to study the sorption kinetics, thermodynamics, and equilibrium isotherms of TC with Fe_3O_4 NP@TOMATS IL. The results showed that the maximum removal efficiency of TC in optimum conditions of pH (7), contact time (90 min), adsorbent dosage (0.2 mg L^{-1}), temperature (328 K), and initial concentration of TC (30 mg L^{-1}) was obtained 92% and 73% in the synthetic and real samples, respectively. Examination of the kinetics and adsorption isotherm equations demonstrated that the adsorption process followed the pseudo-second-order and the Freundlich isotherm. Also, the amount of equilibrium adsorption capacity is 36 mg g^{-1} in the real sample. Investigation of thermodynamic equations revealed that the adsorption by iron oxide nanoparticles modified with TOMATS IL was physically and spontaneously endothermic. The results obtained from the experiments also indicated that the synthesized nanocomposite has high reusability and recyclability after four periodic cycles.

Keywords: Tetracycline; Iron oxide nanoparticles; Ionic liquid; TOMATS

1. Introduction

The existence of antibiotics in the environment, including water, has raised public concern. Tetracycline (TC) is one of the most widely used antibiotics in the β-lactam group that belongs to the penicillin group and is used in medicine and veterinary medicine to treat systemic gastrointestinal and bacterial infections [1]. As the name implies, TC contains four cyclic rings with three different groups [2]. It is known as a hard-to-digest compound and remains as active and non-metabolized compounds in the urine and feces of consumers [3]. Properties of antibiotics include low biodegradability, high toxicity, possible carcinogenicity and mutagenicity of DNA, lymphocyte damage, increased human allergy, the spread of antibiotic-resistant bacteria, and unpredicted adverse effects on humans and animals [4]. Various methods have been presented for removal of antibiotics from water and wastewater, including physical processes such as membrane filtration [5], adsorption [6–9], and reverse osmosis [10]; biological methods [11]; chemical methods such as electrocoagulation [12]; and advanced oxidation processes [13–26] such as electro-Fenton [27], (UV/

* Corresponding author.

H_2O_2/O_3) [28], and photocatalytic degradation [29]. The surface adsorption technique, which is one of the most effective methods for water and wastewater treatment, has been considered by researchers due to its simple design, ease of management, high efficiency, less sludge production, environmental adaptation, and the use of inexpensive and available adsorbents [18].

Magnetic nanoparticles are widely used in environmental disinfection due to their small size, low toxicity, and easy separation [17]. Iron oxides have been highly regarded due to their various properties such as non-toxicity, chemical stability, color variation (yellow, orange, red, brown to black), magnetic properties, and low price. Iron is one of the world's most widely used elements due to its easy synthesis and low purification cost [30]. These particles also have high environmental adaptation and reduce secondary contamination. Another advantage of using magnetic nanoparticles is that they are adsorbed by an external magnetic field, which makes them suitable for sample extraction in chemical analysis because it is not necessary to centrifuge and filter the sample after the extraction process. This is probably the most important advantage of magnetic nanoparticles over other nanoparticles [31]. Iron oxide nanoparticles are among the most commonly used magnetic materials, widely incorporated in many fields such as water and wastewater treatment [32].

Ionic liquids (IL) have been employed as a chemical compound with COO–, SH, and amine functional groups to modify some sorbents [33]. The properties of these liquids include their potential to design compounds for specific tasks [34]. The IL used in this plan is trioctylmethylammonium thiosalicylate (TOMATS) IL whose molecular structure is illustrated in Fig. 1 [35].

To remove organic and inorganic pollutants from aqueous media, the following magnetic nanoadsorbents have been used like glutaric anhydride functionalized Fe_3O_4@SiO_2 magnetic nanoparticles [36], chitosan adsorbents modified with Fe_3O_4 [37], activated carbon modified with magnetic Fe_3O_4 nanoparticle composite [38], Fe_3O_4/HAp magnetic nanoparticles [39], Fe_3O_4/SiO_2/CTAB–SiO_2 mesoporous [40], magnetic Fe_3O_4/red mud-nanoparticles [41], magnetic graphene oxide [42], Fe_3O_4/activated montmorillonite nanocomposite [43]. Given the studies conducted, Fe_3O_4@TOMATS IL has not been used to remove TC from aquatic environments so far. In this study, by synthesizing and modifying the Fe_3O_4 NP surface using the TOMATS liquid as a new magnetic nanoadorbent, the best interaction between the contaminant and adsorbent was performed, and the effective parameters in this process were optimized and investigated.

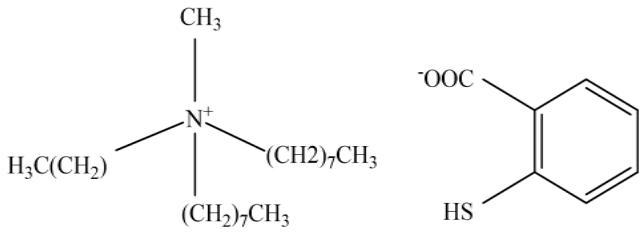

Fig. 1. Molecular structure of TOMATS IL [21].

2. Materials and methods

2.1. Chemicals

The antibiotic standard TC, iron(III) chloride hexahydrate, iron(II) chloride tetrahydrate, trioctyl methyl ammonium chloride (Aliquat, Sigma-Aldrich, USA), thiosalicylic acid, sodium hydroxide, sodium hydrogen carbonate, and ethanol with high purity were purchased from Merck Co., (Germany).

2.2. IL synthesis

To this end, 10 g of thiosalicylic acid (0.065 M) was dissolved in 45–50 mL of 10% wt. of sodium hydrogen carbonate and, then, 1 M of trioctyl methyl ammonium chloride (Aliquat 336, Sigma-Aldrich, USA) was added to the above solution which was approximately 30 mL. The resulting mixture was stirred at a high speed for 1 h by a magnetic stirrer. During this time, the upper phase of the mixture, which was colorless Aliquat 336 (Sigma-Aldrich, USA), was transformed into a green viscous liquid, which is the same as TOMATS IL. After removing the IL from the aqueous phase, it was washed four times with distilled water in a separatory funnel. Finally, a centrifuge machine was used to separate the water from IL. To dry and remove the impurities, it was placed in a vacuum oven at 30°C for 24 h.

2.3. Preparation and characterization of Fe_3O_4@TOMATS IL

First, 36 mM (10 g) of $FeCl_3{\cdot}6H_2O$ and 18 mM (3.67 g) of $FeCl_2{\cdot}4H_2O$ were mixed with the 1:2 stoichiometric ratio from Fe^{2+} to Fe^{3+} and dissolved in 150 mL of deionized water. Then, the solution obtained was completely dissolved using a magnetic stirrer. At 333 K, ammonium hydroxide (NH_4OH) solution was added dropwise to alkalize the solution using a burette in order to achieve a black suspension, indicating magnetic iron nanoparticles. After 10 min of continuous stirring to remove ammonia from the reaction medium, by placing a 1.4 Tesla magnetic magnet under the reaction container, the iron nanoparticles were collected at the bottom of the container. Then, the supernatant was removed and the precipitate obtained was washed three times with deionized water. To modify magnetic nanoparticles with IL, 10 mL of ethanol was added to 0.1 mL of IL in the beaker. The solution obtained contained 10 mg L^{-1} of the IL. Subsequently, 0.5 g of the nanoparticle was weighed and poured into the beaker. Next, the IL solution was poured until covering it. It was placed on the stirrer for 15 min and centrifuged for 15 min. Then, the nanoparticles collected at the bottom of the tube were separated from the supernatant, repeated twice, and finally placed in the oven at 318 K for 5 h to properly dry. It was then used as an adsorbent (iron oxide nanoparticles modified with IL). Adsorbent properties were found by X-ray diffraction (XRD) analysis, surface area determination, volume, cavity size, and porosity distribution Brunauer–Emmett–Teller (BET), Barrett–Joyner–Halenda (BJH), field-emission scanning electron microscopy (FE-SEM), and Fourier-transform infrared (FTIR). The surface morphology of Fe_3O_4@TOMATS IL was observed using a scanning electron microscopy (SEM, PHILIPS XL-30, Eindhoven, Netherlands) at 25 keV. The

energy-dispersive X-ray spectroscopy technique (EDS, PHILIPS XL-30, Eindhoven, Netherlands) was also used to characterize the adsorbent elemental composition. An X-ray diffractometer (Quantachrome NOVA 2000, United States) was applied to identify the XRD pattern of Fe_3O_4@TOMATS IL by using a graphite monochromatic copper radiation (Cu Kα, λ = 1.54 Å) in the region of 10°–70° at 25°C. The specific surface area and pore volume of Fe_3O_4@TOMATS IL were measured by the (BET, Quantachrome NOVA 2000, United States) using N_2 adsorption–desorption isotherms at 77.3 K. In addition, a vibrating sample magnetometer (VSM, 7400, Lakeshare, USA) was employed to determine the magnetic properties of the catalyst in the magnetic field of ±10 kOe at 25°C. The functional groups on the nanoparticles were determined by FTIR spectroscopy (Bruker Alpha spectrometer, United States). Specific surface area and pore size distribution were calculated by the BET equation and the BJH method, respectively.

The TC stock solution at the concentration of 500 mg L^{-1} was used to make the required concentrations (10, 20, 30, 40, and 50 mg L^{-1}). Sampling and testing were performed according to standard water and wastewater methods and each experiment was repeated three times. The influence of pH (3, 7, and 9), contact time (30, 60, 90, and 120 min), adsorbent dosage (0.08, 0.1, 0.15, 0.2, and 0.25 g), and tetracycline (TC) concentration (10, 20, 30, 40, and 50 mg L^{-1}) on process efficiency was investigated, and optimum adsorption conditions were determined. At each stage of the experiment, one parameter was kept variable and the others were kept constant. The efficiency of TC removal in the real wastewater samples of hospital wastewater (Bahonar Hospital Wastewater, Kerman, Iran) was investigated in optimum conditions. The quality features of the real sample are shown in Table 1.

As the concentration of TC in the wastewater was very low and indistinguishable, 30 mg L^{-1} of TC was added to the hospital wastewater. HCl and 0.1 N NaOH were used to adjust pH.

2.4. pH point of zero charge (pH_{PZC}) measurements

pH_{zpc} indicates the scattering state of the electric charge at the adsorbent surface. For determining pH_{zpc}, 0.01 M of NaCl as the electrolyte and 0.1 M of NaOH and hydrochloric acid were used as the control agents. Moreover, 30 mL (per Erlenmeyer flask) of the electrolyte solution was poured into 6 Erlenmeyer flasks of 50 mL and the pH of the solutions was adjusted from 2 to 12 using acid and sodium. A mass of 0.2 g of adsorbent was added to each Erlenmeyer flask. The Erlenmeyer flasks were placed on the shaker at 120 rpm for 1 h and, after the above-mentioned time was spent, the final pH of the Erlenmeyer flask contents was read after filtering using a pH meter. After plotting the pH change curve vs. initial pH, pH_{zpc} was determined.

Table 1
Bahonar Hospital wastewater quality features

Parameter	Amount of (value)
Biochemical oxygen demand	261 mg L^{-1}
Chemical oxygen demand	420 mg L^{-1}
Total suspended solids	19 mg L^{-1}
Total dissolved solids	545 mg L^{-1}
TC	1.12 mg L^{-1}
pH	7.1

2.5. Analysis method

The solution pH was measured with a Hanna pH meter using a combined glass electrode. The concentration of TC was determined by high-performance liquid chromatography (HPLC) (Waters E600, USA). The HPLC analysis equipped with a UV absorbance detector at the wavelength of 272 nm and a c 18 column with 5 μm particles, 250 mm in length and 4.6 mm in internal diameter. The mobile phase was a mixture of water/methanol/acetonitrile/1% acetic acid (15/15/20/50, V/V), flow rate was set at 0.5 mL min^{-1} and 60 μL injections were used.

2.6. Experimental procedures

Antibiotic adsorption experiments were conducted at room temperature according to batch methods. The measurements were performed by mixing a certain amount of the adsorbent with the antibiotic solution in 100 mL flasks, and the mixture was shaken on an automatic shaker (IKA/KS 130 basic, IKA, Germany) at 560 rpm for a fixed period. At the end of the adsorption experiments, the adsorbents were separated by an external magnet.

The pH values were adjusted to the required value by adding negligible volumes of 0.1 or 0.01 mol L^{-1} HCl or NaOH solution.

The equilibrium adsorption capacity (q_e) which expresses the amount of the adsorbed TC on the magnetic nanoadsorbent was calculated by Eq. (1) [47].

$$q_e = \frac{\left(C_0 - C_t\right)V}{m} \tag{1}$$

where C_0 and C_t are the TC concentration (mg L^{-1}) at time 0 and t, V is the volume of the solution (L), and m is the mass of dry magnetic nanoadsorbent used (g). The removal efficiency of TC was calculated using Eq. (2) [48].

$$R = \frac{C_0 - C_e}{C_0} \times 100 \tag{2}$$

2.7. Reaction of isotherms, kinetic, and thermodynamic studies

To determine the equilibrium constant, Erlenmeyer flasks containing 50 mL of TC solution with concentrations of 10, 50, 100, 150, and 200 mg L^{-1} and 0.2 g adsorbent dosage were placed on the mixer for 120 min. To investigate the reaction kinetics, pseudo-first-order and pseudo-second-order equations were used. Langmuir and Freundlich's equations were used to investigate the reaction isotherms. For the thermodynamic examination, the above conditions were studied at 298, 308, and 328 K. The data were analyzed using descriptive statistics and Excel charts.

3. Results and discussion

3.1. Surface morphology and structural analyses

3.1.1. FE-SEM analysis

The results FE-SEM analysis are given in Fig. 2 for the synthesized Fe_3O_4@TOMATS IL nanoparticles.

As seen in Fig. 2a, the crystalline and discrete structures were uniform and spherical and had a minimum rate of agglomeration formed from the nanoparticles. During the modification step of the iron oxide nanoparticles with the TOMATS IL, the properties of the synthesized nanostructures were preserved. In the FE-SEM figure of the synthesized Fe_3O_4@TOMATS IL particles, the particle size was estimated at ~20–40 nm. In addition, the spherical structure and uniformity of the particles were well observed (Fig. 2b).

3.1.2. EDS and mapping analysis

The results of the adsorbent component by EDS analysis and the images related to the adsorbent constituent distribution by EDS-mapping analysis are presented in Fig. 3a and b, respectively.

The EDS analysis demonstrated the highest values of Fe and O with weight percent of 77.1 and 19.2, respectively. The estimated weight percent for iron was also proportional to the volume used in the synthesis experiments. The minor peaks related to some other elements, such as S and Br, in this analysis, indicated minor impurity in the synthesized adsorbent structure, the main origin of which can be attributed to the active TOMATS IL used. EDS mapping was performed to determine the elemental distribution of Fe_3O_4@TOMATS IL (Fig. 3b). According to Fig. 3b, Br, S, Fe, O, and C had a homogeneous distribution, indicating the high uniformity of the prepared Fe_3O_4@TOMATS IL.

3.1.3. XRD analysis

The results of the XRD spectrum of Fe_3O_4@TOMATS IL are displayed in Fig. 4.

According to the results of XRD, the crystalline structure of Fe_3O_4 was preserved after adding IL, and 2θ: 35.624, 62.816 of O and the Fe structures were identified. The highest peaks at angles, 35.624, 57.22, and 62.816 were equal to 857, 230, and 365 indices, respectively, which approved the existence of Fe_3O_4 cubic crystals compared with the standard (98–011–1282.JCPDS NO) presence of crystals. The cube confirmed the shape of Fe_3O_4.

3.1.4. Specific surface area analysis, cavity volume and size distribution (BET and BJH)

The specific surface area, volume, and size distribution analysis of the cavities on Fe_3O_4@TOMATS IL based on adsorption and desorption isotherms of nitrogen gas at 350.3 K (gas boiling point of N_2 at the atmospheric pressure) as well as the range of pressure ratio 1–0.5 were calculated and are illustrated in Figs. 5a and b.

The results of BET and BJH analyses for determining surface area, volume, cavities' size distribution, and porosity were as follows: The specific surface area measured from Fe_3O_4@TOMATS IL was 69.696 $m^2 g^{-1}$ using BET analysis and 78.174 $m^2 g^{-1}$ by BJH analysis, which was larger than the Fe_3O_4 NP (56 $m^2 g^{-1}$) reported. The mean diameter of the cavities was obtained as 17.234 and 4.68 using BET and BJH analyses, respectively.

3.1.5. FTIR analysis

The results of FTIR analysis for Fe_3O_4 nanoparticles (a), TOMATS IL (b), and Fe_3O_4 and TOMATS IL (c) are shown in Fig. 6, respectively.

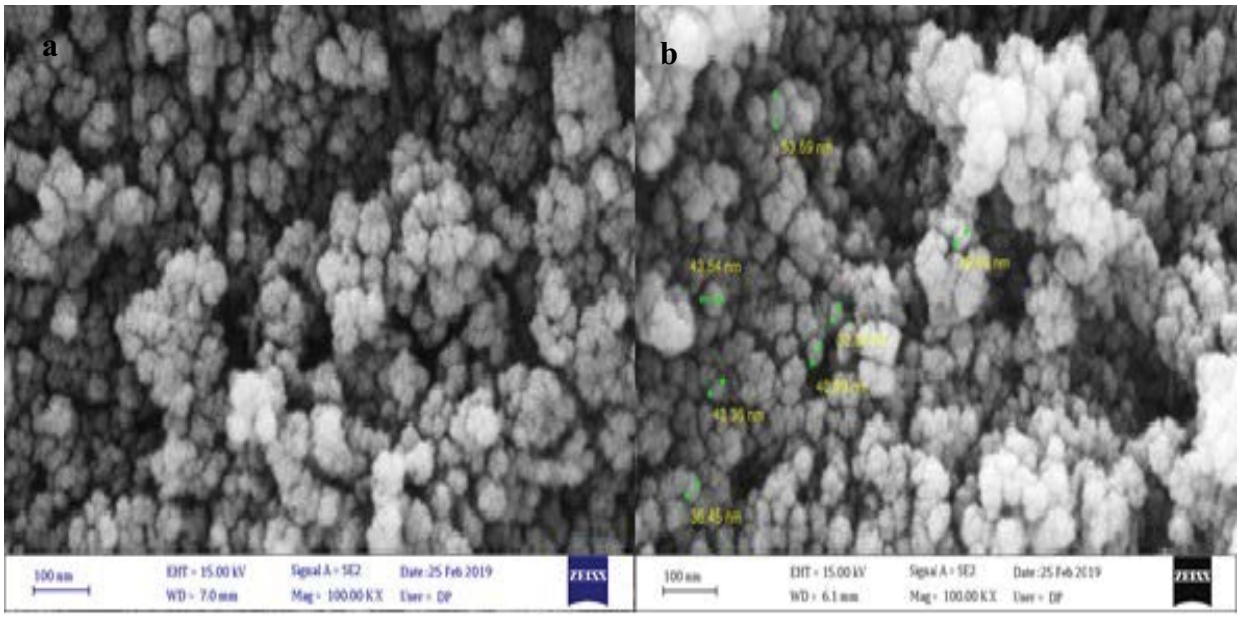

Fig. 2. Field-emission scanning electron microscopy images of synthesized (a) Fe_3O_4 and (b) Fe_3O_4 and IL.

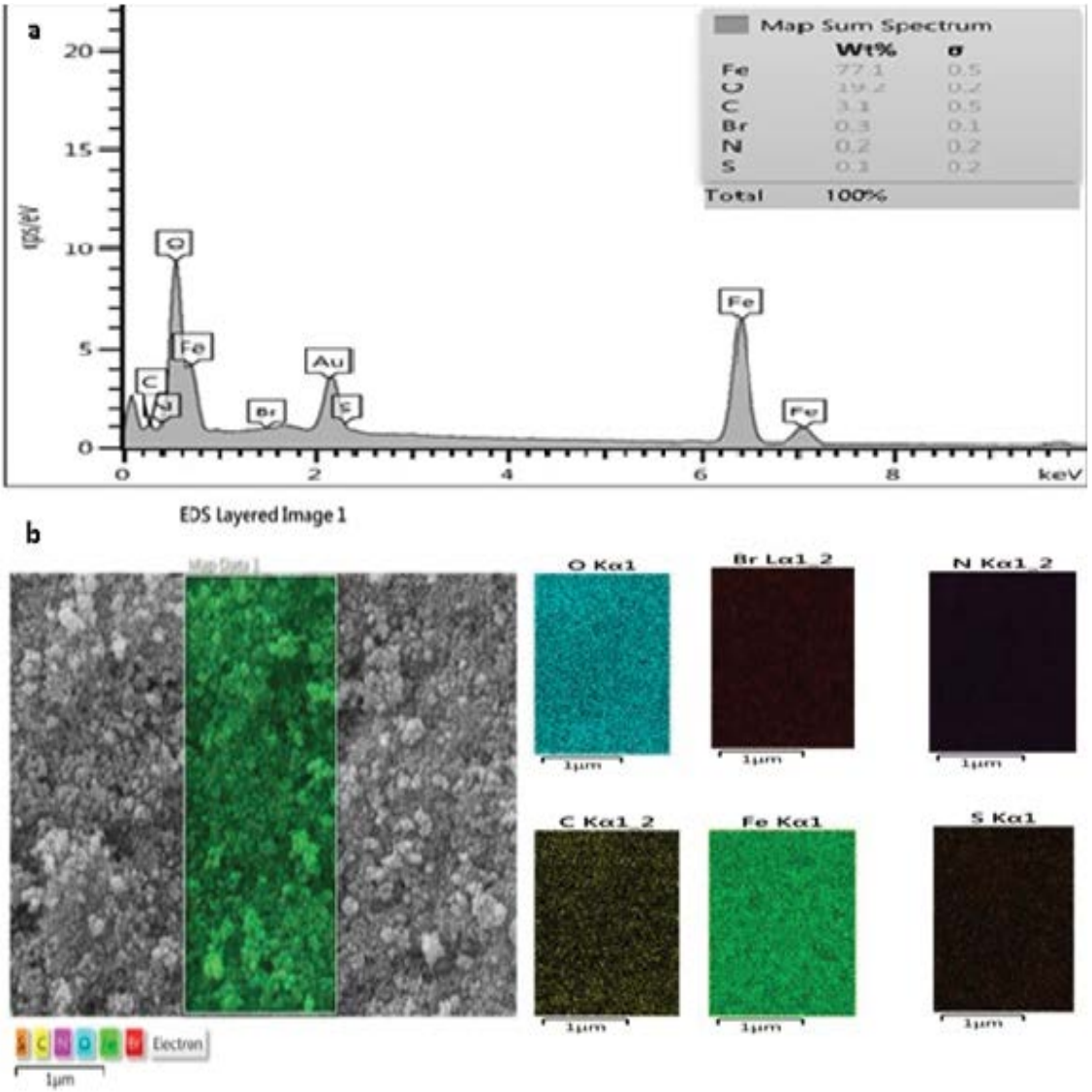

Fig. 3. (a) EDS patterns and (b) elemental mapping images of the as-prepared of Fe_3O_4@TOMATS IL.

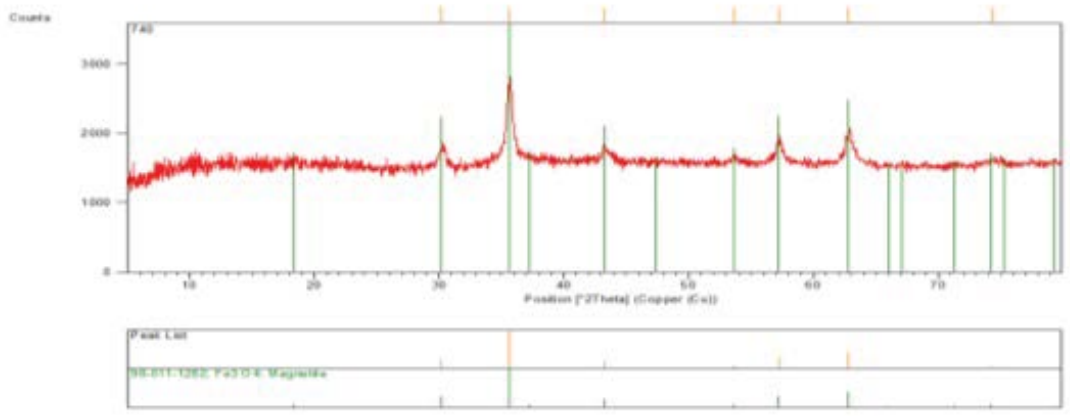

Fig. 4. X-ray diffraction spectrum.

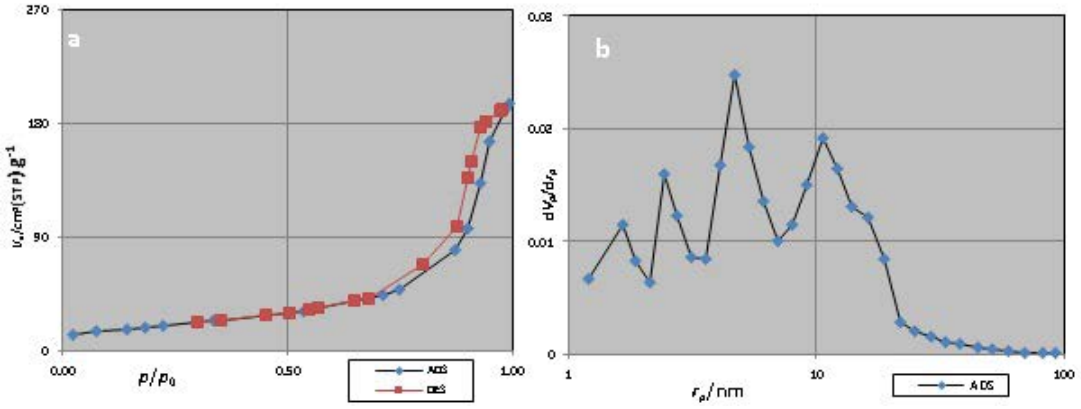

Fig. 5. Specific surface area analysis, volume and size distribution of cavities on Fe_3O_4 and IL using (a) BET and (b) BJH theories.

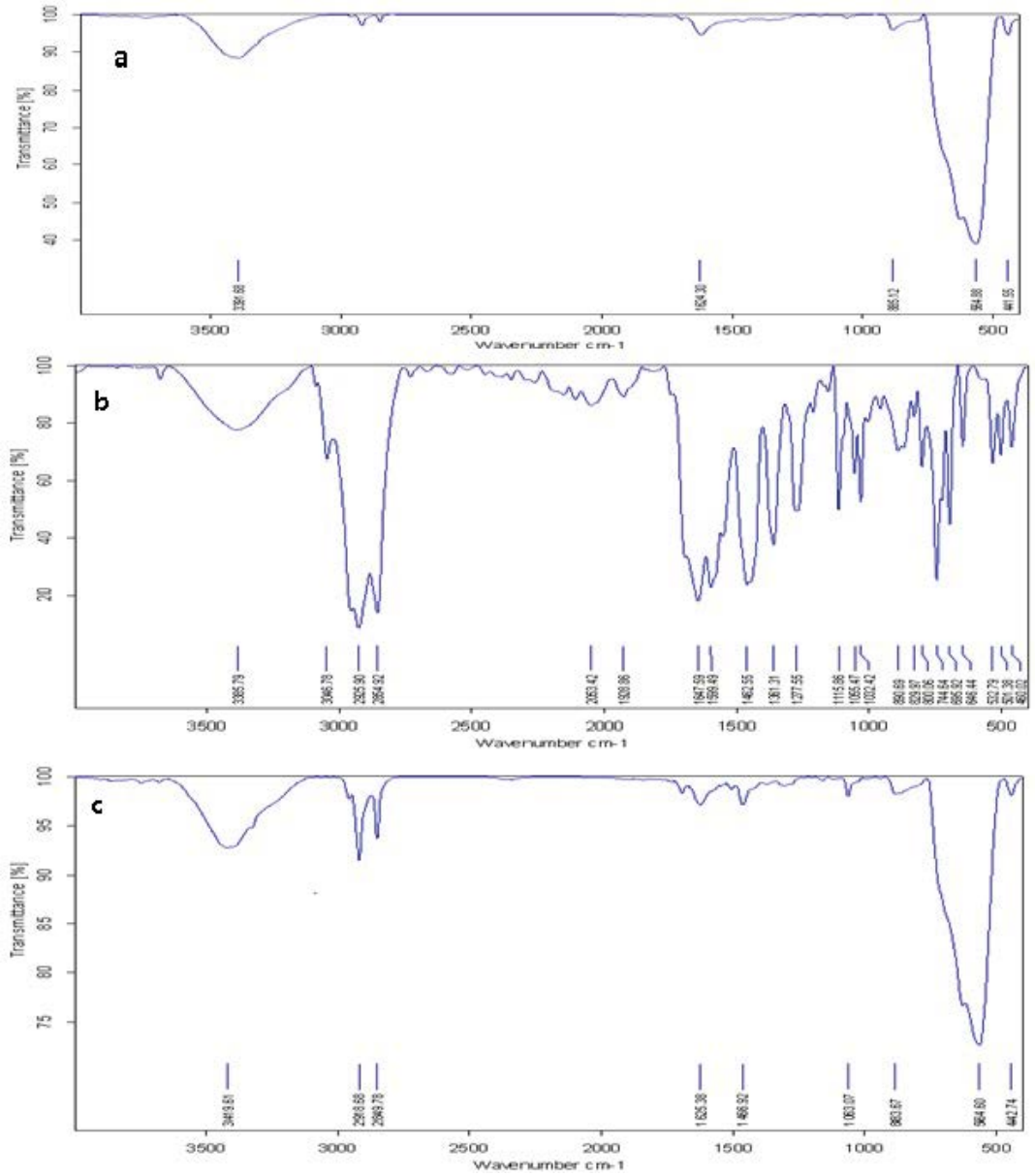

Fig. 6. Results of (a) FTIR analysis for Fe_3O_4, (b) TOMATS IL and (c) Fe_3O_4 and IL.

In Fig. 6c, the adsorption peak at 564.60 cm^{-1} can be attributed to the stretching vibration of Fe–O. In Fig. 6b, the adsorption peaks at 3,419.61 cm^{-1} were related to the stretching vibration of the OH groups, –2,918.65^{-1} to COO and $–CH_2$, 1,647.59 cm^{-1} to C=O, 1,462.55 cm^{-1} to CH_3 and CH_2, and 744.64 cm^{-1} to C–H were the TOMATS IL molecules and confirmed the IL structure. In Fig. 6c, two adsorption bands of 2,918.65 and 2,849.78 cm^{-1} indicated that the IL structure on Fe_3O_4 occurred successfully.

3.2. Adsorption experiments

3.2.1. Effect of pH and contact time

The effect of time and pH on antibiotic removal efficiency is shown in Fig. 7.

The removal percentage was increased by increasing pH from 3 to 7 and reached maximum removal at pH = 7. Then, the removal percentage decreased slightly by increasing the pH from 7 to 9. The removal percentage of TC increased as the contact time rose to 90 and 120 min and then reached equilibrium. The highest adsorption efficiency for the Fe_3O_4@TOMATS IL adsorbent was about 92%. Studies have shown that the decrease and increase in TC removal efficiency at acidic and alkaline pH can be attributed to the two parameters of pK_a and pH_{ZPC} [44]. TC molecules have hydroxyl, carbonyl, amide, and amine functional groups with pK_a of 3.3, 7.7, and 9.7. When pH < 3.3, TC is positively charged due to the uptake of H^+ in acidic conditions and the formation of dimethyl ammonium groups. When 3.3 < pH < 7.7, the TC is zwitterion (bipolar). Finally, at pH > 7.7, TC is anionic in the environment due to the loss of proton of some functional groups [37]. As a result, the adsorption mechanism is probably either due to the lack of electrical repulsion force between the adsorbent surface and the TC molecules having both benzene rings and bond pairs (C = C, C = C), or the hydrophobic force between TC and the adsorbent [45]. In the study by Majidi et al. [46] on the efficiency of the Sono-Electro-Fenton process for the removal of ciprofloxacin antibiotics from aqueous solutions, it was found that the Sono-Electro-Fenton process at pH = 3 had the highest efficiency of ciprofloxacin removal (97%). In the study by Liu et al. [47], the removal of antibiotics sulfamethazine and sulfamethoxazole from aqueous solutions was investigated with hexadecyl trimethyl ammonium modified with activated carbon, in which the maximum removal efficiency at pH = 7–5 was 85.24% [47]. Samadi et al. [48] study in Hamadan, Iran, on the removal of nickel from aqueous solutions using multi-wall carbon nanotubes showed that the removal efficiency increased from 5 to 10 by increasing the pH of the solution. This was because by increasing the pH, the surface charge of the carbon nanotubes became more negative, which resulted in electrostatic reactions and, thus, better adsorbed positive charge metal ions such as nickel.

3.2.2. Effect of initial concentration

The effect of initial TC concentration on removal efficiency is shown in Fig. 8.

The percentage of TC removal increased (88%) by increasing the initial concentration to 30 mg L^{-1} and then decreased. In other words, under optimal conditions, the amount of TC adsorbed on the adsorbent decreased as the initial TC concentration increased. This phenomenon was because at low concentrations, the ratio of the available surface area to initial TC concentration was high and, therefore, the adsorption efficiency of TC also increased. At high concentrations, the adsorption efficiency decreased as this ratio decreased. The results obtained by Lu et al. [49] on adsorption were consistent with those of the study performed by hexavalent chromium with carbon-based adsorbents obtained from biological waste. The results were consistent with those of Ghodrat et al. [37] who compared the efficiency of adsorbents, including chitosan and chitosan modified with Fe_3O_4, in the removal of erythromycin from aqueous media. The results were also consistent with those of Khoshnamvand et al. [50] who performed ciprofloxacin adsorption using manganese oxide nanoparticles as the adsorbent.

3.2.3. Effect of adsorbent dosage

Fig. 9 demonstrates the effect of adsorbent dosage on the removal rate of TC antibiotics using Fe_3O_4@TOMATS IL.

By increasing the adsorbent content from 0.08 to 0.2 g, the removal of TC for constant concentration from TC was

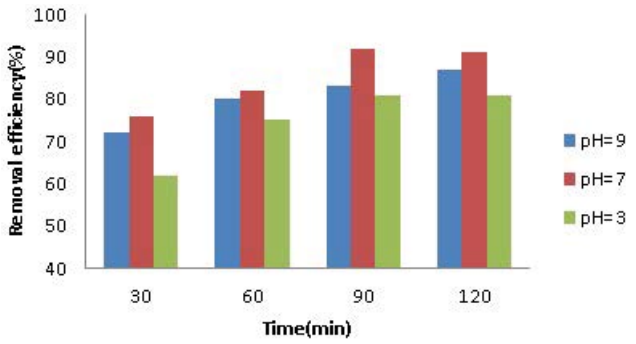

Fig. 7. Time and pH effect on removal efficiency (adsorbent content = 0.2 mg L^{-1}; temperature = 328 K; initial dosage of TC = 30 mg L^{-1}).

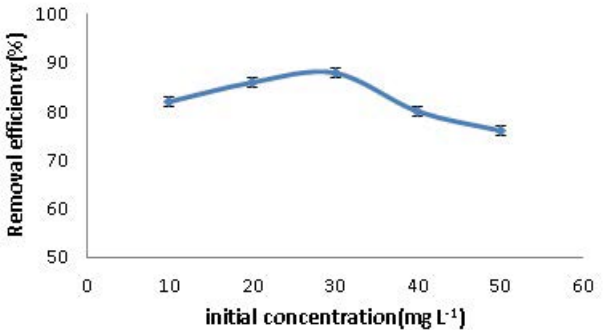

Fig. 8. Effect of initial TC concentration on removal efficiency (pH = 7; contact time = 90 min; adsorbent dosage = 0.2 mg L^{-1}; temperature = 328 K).

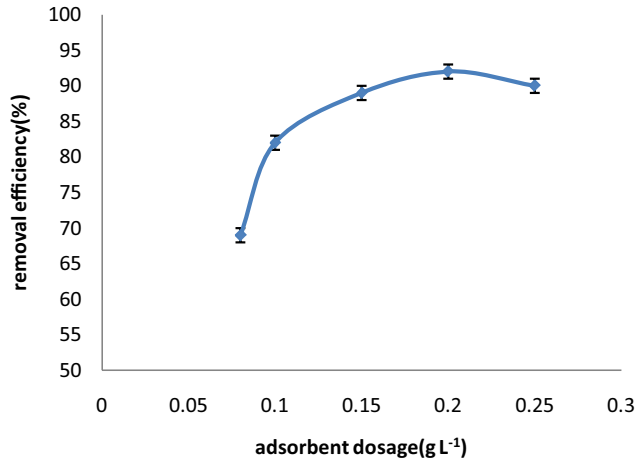

Fig. 9. Effects of adsorbent dosage on removal efficiency (pH = 7; contact time = 90 min; temperature = 328 K; initial concentration of TC = 30 mg L^{-1}).

increased (92%), while it decreased after 0.2 g of concentration with a slight gradient. The experimental results showed that the optimal adsorbent measured for TC removal was 0.2 g. In general, increasing the amount of adsorption due to the increased adsorbent consumption could be attributed to greater access to the surface active sites and the numerous adsorbent vacancies [51]. In the study conducted by Alidadi et al. [52] in Iran on the adsorption of ciprofloxacin HCl from aqueous solutions by adsorption on the chitosan/zeolite composite, it was found that the adsorption of ciprofloxacin increased with the adsorbent dose. By investigating the adsorption of metronidazole on activated carbon modified with the nanoparticles of iron zero, Wang found that the removal efficiency increased with the adsorbent dose [53]. It is noteworthy that the specific surface area available for the adsorbent molecules at low adsorbent levels was lower than the higher adsorbent contents; therefore, fewer adsorbent molecules could be adsorbed on the adsorbent. However, by increasing the content of the specific surface area of the adsorbent available to the adsorbed molecules, more molecules of the adsorbed material can be adsorbed onto the adsorbent. It is also important to note that when the number of molecules adsorbed in the solution was constant, an increase in the content of adsorbent actually gave more active sites to the adsorbed molecules and provided a greater chance of being adsorbed; consequently, the process efficiency was enhanced [54].

3.2.4. Effect of temperature

Fig. 10 shows the effect of temperature on the removal rate of TC using Fe_3O_4@TOMATS IL.

The removal percentage of TC increased (91%) as the temperature increased. The results revealed that the adsorbent surface adsorption process was generally carried out as endothermic. As a result, the optimum temperature for the removal of TC was 328 K. Therefore, the removal percentage for TC increased with temperature, which increased the movement of the adsorbed particles and their probable collision with the adsorbent surface. Also, by increasing the

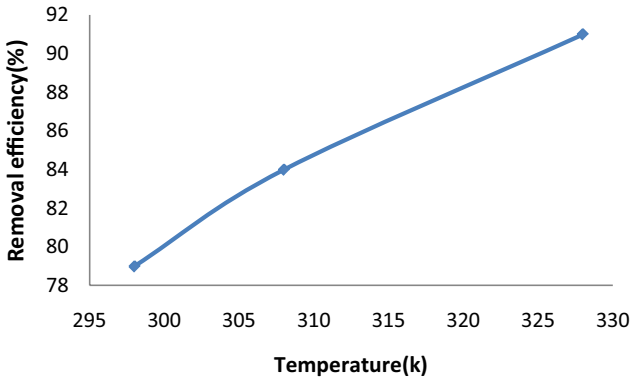

Fig. 10. Effects of temperature on removal efficiency (pH = 7; contact time = 90 min; adsorbent dosage = 0.2 mg L^{-1}; initial concentration of TC = 30 mg L^{-1}).

temperature, the reaction activation energy and reaction rate also increased. In addition, with increasing temperature, the chemical absorption capacity decreased, while the physical absorption capacity increased [55]. The results were consistent with those of Sharma et al. [56] investigation on the kinetic and thermodynamic studies of ciprofloxacin adsorption from aqueous solutions using copper oxide nanoparticles. The results were also in line with those of Mao et al. [57] examining ciprofloxacin adsorption using a magnetic carbon composite.

3.3. Adsorption kinetics

The adsorption rate is an important parameter to evaluate the adsorption process as a full-scale adsorption plant. The pseudo-first-order and pseudo-second-order kinetic models were used to estimate the rate of the adsorption process. Pseudo-first-order and pseudo-second-order kinetic models can be respectively expressed by Eqs. (3) and (4) [43,58].

$$\mathrm{Ln}\left(q_e - q_t\right) = \mathrm{Ln}\, q_e - k_1 t \tag{3}$$

where q_e and q_t are the amount of TC adsorbed onto the adsorbent (mg g^{-1}) at equilibrium at t, respectively, and k_1 (min^{-1}) is the rate constant of the pseudo-first-order adsorption model.

$$\frac{t}{q_t} = \frac{1}{k_2 q_e^2} + \frac{1}{q_e} \times t \tag{4}$$

where k_2 (g mg min^{-1}) is the rate constant of the pseudo-second-order adsorption model. Figs. 11a and b depicts the reaction kinetics first-order and second-order of TC adsorption by Fe_3O_4@TOMATS IL.

Table 2 shows the pseudo-first-order and second-order kinetic parameters for TC.

The pseudo-second-order kinetics model with correlation coefficients of 0.9963 described the surface adsorption process more accurately. It involved all the surface adsorption steps and well described the surface adsorption mechanism. In second-order kinetics, two reactions were assumed

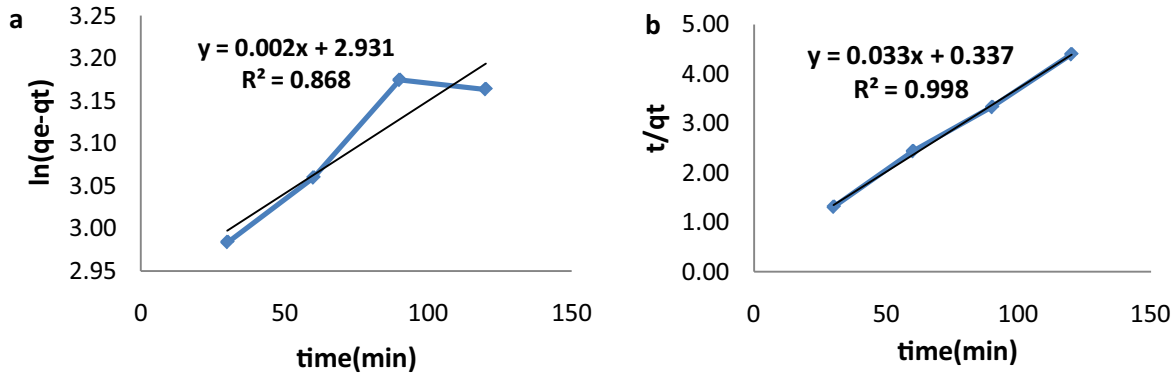

Fig. 11. Reaction kinetics (a) first-order and (b) second-order of TC adsorption by Fe_3O_4@TOMATS IL.

to occur; one of these reactions occurred rapidly and reached equilibrium, whereas the other happened slowly and could last for long periods of time [59,60]. In the study conducted by Peng et al. [61] in China on studying the behavior and mechanism of ciprofloxacin adsorption from bamboo-carbonated aqueous solutions, it was found that the adsorption process followed pseudo-second-order kinetics. The results were in line with those of Khoshnamvand et al. [50] on studying the adsorption of ciprofloxacin using manganese oxide nanoparticles as adsorbent kinetics process, in which the adsorption process followed pseudo-second-order kinetics.

3.4. Adsorption isotherms

To investigate the adsorption isotherms, Langmuir and Freundlich's equations were employed using Eqs. (5) and (6), respectively:

$$\frac{C_e}{q_e} = \frac{1}{K_L q_m} + \frac{1}{q_m} C_e \tag{5}$$

where K_L (L mg^{-1}) denotes the Langmuir constant related to the rate of adsorption, C_e (mg L^{-1}) is the concentration at equilibrium time of the adsorbate, and q_m (mg g^{-1}) indicates the maximum mass of the adsorbate.

$$\text{Log } q_e = \text{Log } K_F + \frac{1}{n} \text{Log } C_e \tag{6}$$

where n (dimensionless) and K_F (L mg^{-1}) are Freundlich isotherm constants; the value of n provides an indication of the adsorption process favorability which is related to surface heterogeneity and adsorption intensity. In the Freundlich isotherm model, the value of $1/n < 1$ indicates a normal adsorption. On the other hand, $1/n > 1$ is indicative of cooperative adsorption [62].

Figs. 12a and b displays the isotherms Freundlich and Langmuir of TC adsorbed by Fe_3O_4@TOMATS IL.

Table 3 presents the calculations of Freundlich and Langmuir surface adsorption isotherms.

The results showed the Freundlich isotherm model for pH with correlation coefficients (R^2) of 0.922. In addition, the slope value of $1/n$ was in the range of 0 to 1, indicating the desirable process of surface adsorption. Also, $n > 1$ indicates the physicality of the adsorption process as well as a desirable, fast, and easy surface adsorption process [59]. The Freundlich isotherm model under optimal conditions with correlation coefficients (R^2) equal to 0.922 had better compliance than the Langmuir isotherm model with the experimental data. Based on the Freundlich isotherm, the adsorption of TC occurred in a multilayer at a heterogeneous energy level. A study by AL-Othman et al. [63] in Iraq on investigating the adsorption of ciprofloxacin HCl from aqueous solutions by adsorption onto Iraqi porcelinaite showed that the adsorption process followed the Freundlich isotherm [63].

3.5. Adsorption thermodynamics

Eqs. (7)–(9) were used to calculate the thermodynamic parameters:

$$\Delta G^\circ = -RT \ln K \tag{7}$$

where R, T, and K denote the universal gas constant (8.314 J (K mol)$^{-1}$), the absolute temperature (K), and the distribution coefficient, respectively, and ΔG° (kJ mol^{-1}) represents the Gibbs free energy.

Table 2
Pseudo-first-order and pseudo-second-order kinetic parameters of surface adsorption

Pseudo-first-order model			Pseudo-second-order model		
R^2	k_1, (g mg^{-1} min^{-1})	q_e, (mg g^{-1})	R^2	k_2, (g mg^{-1} min^{-1})	q_e, (mg g^{-1})
0.8685	0.0208	3.68	0.9982	0.2187	3.68

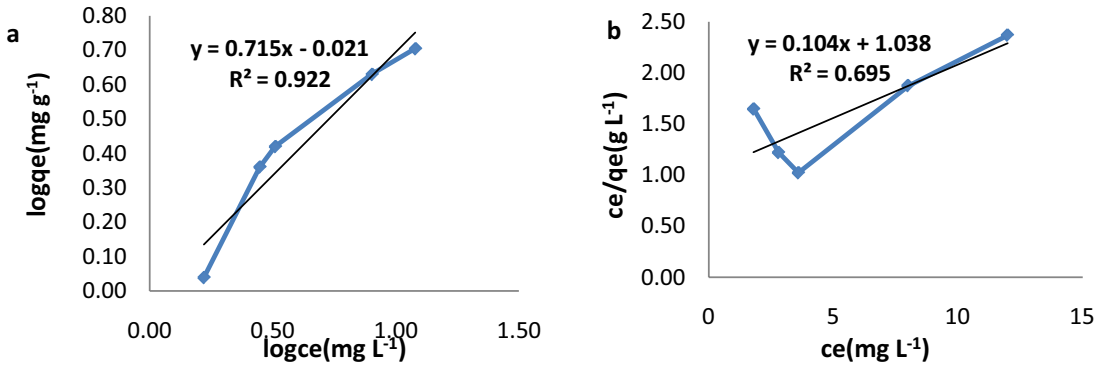

Fig. 12. Isotherms (a) Freundlich and (b) Langmuir for adsorption of TC by Fe_3O_4@TOMATS IL.

$$\Delta G^\circ = \Delta H^\circ - T\Delta S^\circ \tag{8}$$

where ΔH° (kJ mol^{-1}) is the enthalpy of adsorption, and ΔS° (kJ mol^{-1} K^{-1}) is the entropy change.

$$\ln K = \frac{\Delta S^\circ}{R} - \frac{\Delta H^\circ}{RT} \tag{9}$$

ΔH° and ΔS° can be calculated from the slope and intercept of the linear plot of ln$K$ vs. $1/T$.

Table 4 shows the thermodynamic parameters for TC adsorption by Fe_3O_4@TOMATS IL at pH = 7, contact time of 90 min, adsorbent content of 0.2 mg L^{-1}, temperature of 328 K, and initial TC concentration of 30 mg L^{-1}.

According to the results, a negative ΔG° value was obtained and showed that the TC adsorption process was spontaneous. In addition, the positive value of ΔH° indicated the endothermic nature of the adsorption process. The positive value of ΔS° showed that the surface adsorption process of TC on the adsorbent was followed by an increase in disorder. Given $0 < \Delta G^\circ < 0$, the process was physical. The results were consistent with those of Sharma et al. [56] who performed a kinetic and thermodynamic study of ciprofloxacin adsorption from aqueous solutions using copper oxide nanoparticles.

3.6. Recovery and reuse

The effect of adsorbent reuse is illustrated in Fig. 13.

For each usage, the adsorbent was washed and dried using deionized water/ethanol and used for TC adsorption under identical conditions. The results showed that there was a very slight decrease in the adsorption activity using the adsorbent in the second use, and the adsorbent remained substantially constant in the second and third stages of reuse. This slight decrease in the adsorbent activity can be attributed to the occupation of the active sites on the adsorbent and, therefore, the reduction of the bond strength activity between the TC and the adsorbent in each step of adsorption. The results showed 85% removal of TC after four steps of adsorbent usage.

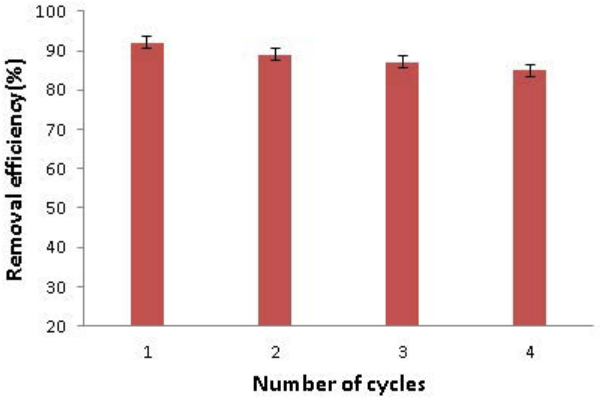

Fig. 13. Diagram of adsorbent recovery and resuscitation (pH = 7; contact time = 90 min; adsorbent dosage = 0.2 mg L^{-1}; temperature = 328 K; initial concentration of TC = 30 mg L^{-1}).

Table 5 compares Fe_3O_4@TOMATS IL adsorbents with a number of adsorbents containing NP Fe_3O_4.

Evidently, less time and high efficiency were the properties of this adsorbent for the removal of TC.

4. Conclusion

The adsorbents were synthesized and investigated in a structural manner. The size of the synthesized particles was

Table 3
Various parameters evaluated for Langmuir and Freundlich adsorption isotherm models

Langmuir				Freundlich		
K_L (mg^{-1})	q_m (mg g^{-1})	R_1	R^2	$1/n$	K_F (mg g^{-1})	R^2
0.1	9.58	0.14	0.6954	0.97851	1.05	0.922

Table 4
Thermodynamic parameters evaluated for adsorption of TC on Fe_3O_4@TOMATS IL

T (K)	ΔG°(kJ mol^{-1})	K	ΔS°(kJ mol^{-1} K^{-1})	ΔH°(kJ mol^{-1})
298	1.715	0.50		
308	0.916	0.70	84.73	26.98
328	0.817	1.35		

Table 5
Comparing Fe_3O_4@TOMATS IL adsorbent properties with a number of adsorbents on Fe_3O_4 basis adsorbents

Adsorbent	Pollutant	Time (min)	Adsorbent dose	Pollutant concentration	Removal efficiency%	References
Fe_3O_4 nanoparticles	Doxorubicin hydrochloride	120	0.02 g	10 mg L^{-1}	80.2	[52]
Chitosan-Fe_3O_4	Erythromycin	50	2 g	10 mg L^{-1}	84	[22]
Fe_3O_4-red mud nanoparticles	Ciprofloxacin (CIPRO)	180	3 g	5 mg L^{-1}	90	[26]
Fe_3O_4 NP@TOMATS IL	TC	90	0.2 g	30 mg L^{-1}	92	This work

estimated to be ~20–40 nm and the spherical structure and uniformity of the particles were well observed. The crystalline structure of Fe_3O_4 was maintained after adding IL, and Fe and O had the highest values of 77.1 % and 19.2% wt., respectively. The adsorption process was the Freundlich isotherm, and the slope value of $1/n$ was in the range of 0 to 1, indicating that the surface adsorption process was desirable. Also, $n > 1$ indicated the physicality of the adsorption process as well as the desirable, fast, and easy surface adsorption process. The kinetics process followed the second-order model. Therefore, the absorbent was environmentally friendly adsorbent and reusable for several times for high-performance TC removal.

Acknowledgments

This research was carried out in the Environmental Health Engineering Research Center of Kerman University of Medical Sciences and was sponsored by the Vice-Chancellor for Research and Technology of said university (Project code: 99000455).

References

[1] N. Le-Minh, S.J. Khan, J.E. Drewes, R.M. Stuetz, Fate of antibiotics during municipal water recycling treatment processes, Water Res., 44 (2010) 4295–4323.
[2] V. Homem, L. Santos, Degradation and removal methods of antibiotics from aqueous matrices – a review, J. Environ. Manage., 92 (2011) 2304–2347.
[3] D.Y. Zhang, J. Yin, J.Q. Zhao, H. Zhu, C.Y. Wang, Adsorption and removal of tetracycline from water by petroleum coke-derived highly porous activated carbon, J. Environ. Chem. Eng., 3 (2015) 1504–1512.
[4] G.Y. Zhang, D.C. Ma, C.N. Peng, X.X. Liu, G.W. Xu, Process characteristics of hydrothermal treatment of antibiotic residue for solid biofuel, Int. J. Chem. Eng., 252 (2014) 230–238.
[5] C. Echaide-Górriz, J.A. Zapata, M. Etxeberría-Benavides, C. Téllez, J. Coronas, Polyamide/MOF bilayered thin film composite hollow fiber membranes with tuned MOF thickness for water nanofiltration, Sep. Purif. Technol., 236 (2020) 116265.
[6] N. Javid, A. Nasiri, M. Malakootian, Removal of nonylphenol from aqueous solutions using carbonized date pits modified with ZnO nanoparticles, Desal. Water Treat., 141 (2019) 140–148.
[7] M. Malakootian, A. Nasiri, H. Mahdizadeh, Preparation of $CoFe_2O_4$/activated carbon@chitosan as a new magnetic nanobiocomposite for adsorption of ciprofloxacin in aqueous solutions, Water Sci. Technol., 78 (2018) 2158–2170.
[8] M. Malakootian, M. Hashemi, A. Toolabi, A. Nasiri, Investigation of nickel removal using poly(amidoamine) generation 4 dendrimer (PAMAM G4) from aqueous solutions, J. Eng. Res. (Kuwait), 6 (2018) 13–23.
[9] N. Amirmahani, H. Mahdizadeh, M. Malakootian, A. Pardakhty, N.O. Mahmoodi, Evaluating nanoparticles decorated on Fe_3O_4@SiO_2-schiff base (Fe_3O_4@SiO_2-APTMS-HBA) in adsorption of ciprofloxacin from aqueous environments, J. Inorg. Organomet. Polym. Mater., (2020), doi: 10.1007/s10904–020–01499–5.
[10] F. Yu, S. Sun, S. Han, J. Zheng, J. Ma, Adsorption removal of ciprofloxacin by multi-walled carbon nanotubes with different oxygen contents from aqueous solutions, Chem. Eng. J., 285 (2016) 588–595.
[11] H. Bagheri, A. Afkhami, A. Noroozi, Removal of pharmaceutical compounds from hospital wastewaters using nanomaterials: a review, Anal. Bioanal. Chem. Res., 3 (2016) 1–18.
[12] S.M. Safwat, Coupling microbial fuel cells with electrocoagulation cells to form an integrated system for wastewater treatment, Pol. J. Environ. Stud., 28 (2019) 1909–1915.
[13] F. Tamaddon, A. Nasiri, G. Yazdanpanah, Photocatalytic degradation of ciprofloxacin using $CuFe_2O_4$@methyl cellulose based magnetic nanobiocomposite, MethodsX, 7 (2020) 74–81.
[14] F. Tamaddon, M.H. Mosslemin, A. Asadipour, M.A. Gharaghani, A. Nasiri, Microwave-assisted preparation of $ZnFe_2O_4$@methyl cellulose as a new nano-biomagnetic photocatalyst for photodegradation of metronidazole, Int. J. Biol. Macromol., 154 (2020) 1036–1049.
[15] M. Malakootian, H. Mahdizadeh, M. Khavari, A. Nasiri, M.A. Gharaghani, M. Khatami, E. Sahle-Demessie, R.S. Varma, Efficiency of novel Fe/charcoal/ultrasonic micro-electrolysis strategy in the removal of Acid Red 18 from aqueous solutions, J. Environ. Chem. Eng., 8 (2020) 103553.
[16] M. Malakootian, M. Khatami, H. Mahdizadeh, A. Nasiri, M. Amiri Gharaghani, A study on the photocatalytic degradation of *p*-nitroaniline on glass plates by thermo-immobilized ZnO nanoparticle, Inorg. Nano-Metal Chem., 50 (2020) 124–135.
[17] A. Nasiri, F. Tamaddon, M.H. Mosslemin, M.A. Gharaghani, A. Asadipour, New magnetic nanobiocomposite $CoFe_2O_4$@methylcellulose: facile synthesis, characterization, and

photocatalytic degradation of metronidazole, J. Mater. Sci. - Mater. Electron., 30 (2019) 8595–8610.
[18] A. Nasiri, F. Tamaddon, M.H. Mosslemin, M. Faraji, A microwave assisted method to synthesize nano$CoFe_2O_4$@methyl cellulose as a novel metal-organic framework for antibiotic degradation, MethodsX, 6 (2019) 1557–1563.
[19] M. Malakootian, N. Olama, M. Malakootian, A. Nasiri, Photocatalytic degradation of metronidazole from aquatic solution by TiO_2-doped Fe^{3+} nano-photocatalyst, Int. J. Environ. Sci. Technol., 16 (2019) 4275–4284.
[20] M. Malakootian, A. Nasiri, H. Mahdizadeh, Metronidazole adsorption on $CoFe_2O_4$/activated carbon@chitosan as a new magnetic biocomposite: modelling, analysis, and optimization by response surface methodology, Desal. Water Treat., 164 (2019) 215–227.
[21] M. Malakootian, A. Nasiri, M. Khatami, H. Mahdizadeh, P. Karimi, M. Ahmadian, N. Asadzadeh, M.R. Heidari, Experimental data on the removal of phenol by electro-H_2O_2 in presence of UV with response surface methodology, MethodsX, 6 (2019) 1188–1193.
[22] M. Malakootian, A. Nasiri, M.R. Heidari, Removal of phenol from steel plant wastewater in three dimensional electrochemical (TDE) process using $CoFe_2O_4$@AC/H_2O_2, J. Z. Phys. Chem., (2019), doi: 10.1515/zpch-2019–1499.
[23] M. Malakootian, A. Nasiri, A. Asadipour, E. Kargar, Facile and green synthesis of $ZnFe_2O_4$@CMC as a new magnetic nanophotocatalyst for ciprofloxacin degradation from aqueous media, J. Process Saf. Environ., 129 (2019) 138–151.
[24] M. Malakootian, A. Nasiri, A. Asadipour, M. Faraji, E. Kargar, A facile and green method for synthesis of $ZnFe_2O_4$@CMC as a new magnetic nanophotocatalyst for ciprofloxacin removal from aqueous media, MethodsX, 6 (2019) 1575–1580.
[25] M. Malakootian, A. Nasiri, A.N. Alibeigi, H. Mahdizadeh, M.A. Gharaghani, Synthesis and stabilization of ZnO nanoparticles on a glass plate to study the removal efficiency of acid red 18 by hybrid advanced oxidation process (ultraviolet/ZnO/ultrasonic), Desal. Water Treat., 170 (2019) 325–336.
[26] M. Malakootian, K. Kannan, M.A. Gharaghani, A. Dehdarirad, A. Nasiri, Y.D. Shahamat, H. Mahdizadeh, Removal of metronidazole from wastewater by Fe/charcoal micro electrolysis fluidized bed reactor, J. Environ. Chem. Eng., 7 (2019) 103457.
[27] I.R. Bautitz, R.F.P. Nogueira, Degradation of tetracycline by photo-Fenton process—solar irradiation and matrix effects, J. Photochem. Photobiol., A, 187 (2007) 33–39.
[28] I.H. Kim, N. Yamashita, Y. Kato, H. Tanaka, Discussion on the application of UV/H_2O_2, O_3 and O_3/UV processes as technologies for sewage reuse considering the removal of pharmaceuticals and personal care products, J. Water Sci. Technol., 59 (2009) 945–955.
[29] M. Malakootian, H. Mahdizadeh, A. Dehdarirad, M. Amiri Gharghani, Photocatalytic ozonation degradation of ciprofloxacin using ZnO nanoparticles immobilized on the surface of stones, J. Dispersion Sci. Technol., 40 (2019) 846–854.
[30] M. Doltabadi, H. Alidadi, M. Davoudi, Comparative study of cationic and anionic dye removal from aqueous solutions using sawdust-based adsorbent, Environ. Progress Sustainable Energy, 35 (2016) 1078–1090.
[31] P.Y. Wang, X.X. Wang, S.J. Yu, Y.D. Zou, J. Wang, Z.S. Chen, N.S. Alharbi, A. Alsaedi, T. Hayat, Y.T. Chen, X.K. Wang, Silica coated Fe_3O_4 magnetic nanospheres for high removal of organic pollutants from wastewater, Chem. Eng. J., 306 (2016) 280–288.
[32] M. Hua, S.J. Zhang, B.C. Pan, W.M. Zhang, L. Lv, Q.X. Zhang, Heavy metal removal from water/wastewater by nanosized metal oxides: a review, J. Hazard. Mater., 211–212 (2012) 317–331.
[33] X.L. Zhao, Y. Shi, T. Wang, Y. Cai, G.B. Jiang, Preparation of silica-magnetite nanoparticle mixed hemimicelle sorbents for extraction of several typical phenolic compounds from environmental water samples, J. Chromatogr. A, 1188 (2008) 140–147.
[34] S. Keskin, D. Kayrak-Talay, U. Akman, Ö. Hortaçsu, A review of ionic liquids towards supercritical fluid applications, J. Supercrit. Fluids, 43 (2007) 150–180.
[35] K. Dong, X.M. Liu, H.F. Dong, X.P. Zhang, S.J. Zhang, Multiscale studies on ionic liquids, Chem. Rev., 117 (2017) 6636–6695.
[36] W.L. Cai, M.Y. Guo, X.L. Weng, W. Zhang, Z.L. Chen, Adsorption of doxorubicin hydrochloride on glutaric anhydride functionalized Fe_3O_4@SiO_2 magnetic nanoparticles, J. Mater. Sci. Eng. C, 98 (2019) 65–73.
[37] M. Ghodrat, E. Asrari, Comparative study of the performance of chitosan and chitosan adsorbents modified with Fe_3O_4 to eliminate erythromycin from aqueous solutions, Iran. J. Health Environ., 10 (2018) 471–482.
[38] M. Yegane Badi, A. Azari, H. Pasalari, A. Esrafili, M. Farzadkia, Modification of activated carbon with magnetic Fe_3O_4 nanoparticle composite for removal of ceftriaxone from aquatic solutions, J. Mol. Liq., 261 (2018) 146–154.
[39] S. Mohammadi-Aghdam, B. Valinezhad-Saghezi, Y. Mortazavi, S.M. Qhoreishi, Modified Fe_3O_4/HAp magnetically nanoparticles as the carrier for ibuprofen: adsorption and release study, Drug Res. (Stuttg), 69 (2019) 93–99.
[40] R. Zandipak, S. Sobhanardakani, Novel mesoporous Fe_3O_4/SiO_2/CTAB–SiO_2 as an effective adsorbent for the removal of amoxicillin and tetracycline from water, J. Clean Technol. Environ. Policy, 20 (2018) 871–885.
[41] S. Aydin, M.E. Aydin, F. Beduk, A. Ulvi, Removal of antibiotics from aqueous solution by using magnetic Fe_3O_4/red mud-nanoparticles, Sci. Total Environ., 670 (2019) 539–546.
[42] J.H. Miao, F.H. Wang, Y.J. Chen, Y.Z. Zhu, Y. Zhou, S.T. Zhang, The adsorption performance of tetracyclines on magnetic graphene oxide: a novel antibiotics absorbent, Appl. Surf. Sci., 475 (2019) 549–558.
[43] J.L. Chang, J.C. Ma, Q.L. Ma, D.D. Zhang, N. Qiao, M.X. Hu, H.Z. Ma, Adsorption of methylene blue onto Fe_3O_4/activated montmorillonite nanocomposite, Appl. Clay Sci., 119 (2016) 132–140.
[44] D. Avisar, Y. Lester, H. Mamane, pH induced polychromatic UV treatment for the removal of a mixture of SMX, OTC and CIP from water, J. Hazard. Mater., 175 (2010) 1068–1074.
[45] L. Zhang, X.Y. Song, X.Y. Liu, L.J. Yang, F. Pan, J. Lv, Studies on the removal of tetracycline by multi-walled carbon nanotubes, Chem. Eng. J., 178 (2011) 26–33.
[46] S. Majidi, A. Rahmani, M. Samadi, R. Shokoohi, Determination of sono-electrofenton efficiency in removal of ciprofloxacin antibiotic from aqueous solutions, J. Ilam Univ. Med. Sci., 23 (2015) 85–96.
[47] Y. Liu, X.H. Liu, G.D. Zhang, T. Ma, T.Q. Du, Y. Yang, S.Y. Lu, W.L. Wang, Adsorptive removal of sulfamethazine and sulfamethoxazole from aqueous solution by hexadecyl trimethyl ammonium bromide modified activated carbon, Colloids Surf., A, 564 (2019) 131–141.
[48] M.T. Samadi, Z. Kashitarash Esfahani, F. Ahangari, S. Ahmadi, S.J. Jafari, Nickel removal from aqueous environments using carbon nanotubes, J. Water & Wastewater, 24 (2013) 38–44.
[49] A.-H. Lu, E.L. Salabas, F. Schüth, Magnetic nanoparticles: synthesis, protection, functionalization, and application, Angew. Chem. Int. Ed., 46 (2007) 1222–1244.
[50] N. Khoshnamvand, S. Ahmadi, F.K. Mostafapour, Kinetic and isotherm studies on ciprofloxacin an adsorption using magnesium oxide nanopartices, J. Appl. Pharm. Sci., 7 (2017) 79–83.
[51] E. Worch, Adsorption Technology in Water Treatment: Fundamentals, Processes, and Modeling, Walter de Gruyter, Deutsche Nationalbibliothek Publications, Berlin, 2012.
[52] H. Alidadi, M. Dolatabadi, M. Mehrabpour, A. Dehghan, The efficacy of ciprofloxacin removal by chitosan/zeolite composite from aqueous solution: response surface methodology, kinetic and isotherm studies, J. Health Field, 5 (2017) 1–12.
[53] X.Y. Wang, Y. Du, J. Ma, Novel synthesis of carbon spheres supported nanoscale zero-valent iron for removal of metronidazole, Appl. Surf. Sci., 390 (2016) 50–59.
[54] A.A. Babaei, S.N. Alavi, M. Akbarifar, K. Ahmadi, A. Ramazanpour Esfahani, B. Kakavandi, Experimental and modeling study on adsorption of cationic methylene blue dye onto mesoporous biochars prepared from agrowaste, Desal. Water Treat., 57 (2016) 27199–27212.

[55] M.H. Sui, S.C. Xing, L. Sheng, S.H. Huang, H.G. Guo, Heterogeneous catalytic ozonation of ciprofloxacin in water with carbon nanotube supported manganese oxides as catalyst, J. Hazard. Mater., 227–228 (2012) 227–236.
[56] N. Sharma, N. Dhiman, Kinetic and thermodynamic studies for ciprofloxacin hydrochloride adsorption from aqueous solution on Cuo nanoparticles, Int. J. ChemTech Res., 10 (2017) 98–106.
[57] H.X. Mao, S.K. Wang, J.-Y. Lin, Z.S. Wang, J. Ren, Modification of a magnetic carbon composite for ciprofloxacin adsorption, J. Environ. Sci., 49 (2016) 179–188.
[58] D.K. Mahmoud, M.A.M. Salleh, W.A.W.A. Karim, A. Idris, Z.Z. Abidin, Batch adsorption of basic dye using acid treated kenaf fibre char: equilibrium, kinetic and thermodynamic studies, Chem. Eng. J., 181–182 (2012) 449–457.
[59] M.H. Dehghani, M. Alimohammadi, A.H. Mahvi, N. Rastkari, M. Mostofi, M. Gholami, Performance of multiwall carbon nanotubes for removal phenol from aqueous solutions, Iran. J. Health Environ., 6 (2014) 491–502.
[60] R. Arasteh, M. Masoumi, A.M. Rashidi, L. Moradi, V. Samimi, S.T. Mostafavi, Adsorption of 2-nitrophenol by multi-wall carbon nanotubes from aqueous solutions, Appl. Surf. Sci., 256 (2010) 4447–4455.
[61] X.M. Peng, F.P. Hu, F.L.-Y. Lam, Y.J. Wang, Z.M. Liu, H.L. Dai, Adsorption behavior and mechanisms of ciprofloxacin from aqueous solution by ordered mesoporous carbon and bamboo-based carbon, J. Colloid Interface Sci., 460 (2015) 349–360.
[62] D. Chen, Z.Y. Zeng, Y.B. Zeng, F. Zhang, M. Wang, Removal of methylene blue and mechanism on magnetic γ-Fe_2O_3/SiO_2 nanocomposite from aqueous solution, Water Resour. Ind., 15 (2016) 1–13.
[63] Z.A. AL-Othman, R. Ali, Mu. Naushad, Hexavalent chromium removal from aqueous medium by activated carbon prepared from peanut shell: adsorption kinetics, equilibrium and thermodynamic studies, Chem. Eng. J., 184 (2012) 238–247.